Ceramics

Co-firing preparation and properties of piezoelectric ceramic/structural ceramics layered composites

Kan Bian[1,*] , Xiuxiu Li[2,3], Yiping Wang[2,*], Xiongjie Li[2,3], Sheng Sun[2,3], Shuo Feng[2,3], and Ying Yang[2]

[1] School of Materials Science and Engineering, Nanjing Institute of Technology, Nanjing 211167, People's Republic of China
[2] State Key Laboratory of Mechanics and Control of Mechanical Structures, University of Aeronautics and Astronautics, Nanjing 210016, People's Republic of China
[3] College of Materials Science and Technology, University of Aeronautics and Astronautics, Nanjing 210016, People's Republic of China

ABSTRACT

Pb(Zr, Ti)O$_3$(PZT)-based piezoelectric ceramics and Al$_2$O$_3$-based structural ceramics were cast and co-fired to prepare a layered piezoelectric ceramic/structural ceramic composite. Considering the significant differences in sintering characteristics of PZT- and Al$_2$O$_3$-based ceramics, control of the sintering temperature and the dependence of the linear shrinkage on the solid content of the tape-casting films were systematically conducted at first. The sintering density and the interface bonding properties of the prepared composites were then investigated. The results of electrical and mechanical properties of the composite ceramics indicate: By using sintering aids, Al$_2$O$_3$ ceramic could be fully densified and co-fired with PZT ceramic at 1150 °C. Shrinkage matching during sintering was achieved by adjusting the solid contents to 45 vol.% and 65 vol.% for PZT and alumina tape-casting films. In the layered composites, Al$_2$O$_3$ structural ceramic presents an excellent mechanical property with HV hardness of 667, while the PZT functional ceramic presents d_{33}, ε_r and tanδ of 259 pC/N, 965 and 0.37%, respectively.

Introduction

With the rapid development of miniaturization, integration and multifunctionalization of ceramic-based functional devices, it is difficult for ceramic materials with a single function to satisfy the performance requirements. Multifunctional composite ceramic is then becoming more and more interesting and attractive. Up to now, the composite integrating various functional ceramics and the composite including various structural ceramics have been realized. For example, Ryu et al. [1] obtained a

Handling Editor: David Cann.

✥ Springer

composite of two kinds of functional ceramics and fabricated a layered magnetostrictive/piezoelectric composite ceramic by using colloidal bonding method, which exhibited both piezoelectric and magnetostrictive effects. Vincenzo et al. [2] reported the composite composed of Al_2O_3/ZrO_2 ceramic layers by using tape-casting method. However, it is still very challenging to realize the composite of structural and functional ceramics due to the differences in sintering characteristics, which has attracted much attentions in recent years [3].

Layered construction is commonly used in multifunctional ceramic composites. For example, the layered structure can improve the fracture toughness and thermal shock resistance of ceramic materials while maintaining robust intensity [4, 5]. The layered composites usually include these categories: (a) ceramic-based composites [6], (b) ceramic–metal composite materials [7] and (c) ceramic–polymer composite materials [8]. Akedo et al. prepared Pb(Zr, Ti)O_3 (PZT)-based piezoelectric ceramic thick films up to 180 μm on Si, Al_2O_3 and glass substrates by using a supersonic aerosol deposition method. These PZT thick-film composites are potential in applications of piezoelectric actuating, sensing and transducing devices [9–11]. However, the aerosol deposition facility is expensive and the process is largely powder-consuming. Tape-casting and co-firing technology is widely used in layered composites and devices such as multilayer ceramic capacitors with ceramic layer as thinner as several micrometers. To realize the compatible co-fired composite ceramics consisting of different component layers, it is necessary to control the compositions so that the structural ceramic layer and functional ceramic layer have similar sintering temperature. In addition, due to the mismatch of sintering characteristics, the co-fired multilayer functional ceramic will lead to lamination, cracking, warping and other defects in the layered samples after sintering, which are the key obstacles urgently needed to be solved for layered composite ceramic [12]. Differences in sintering shrinkage rate [13], densification rate [14] and thermal expansion rate [15] for different layer components are the main reasons to result in the mismatch during co-fired process. Hence, control of other casting and sintering parameters such as the solid content and debinding is also very critical for the preparation of the composite ceramics.

In this research, a piezoelectric/structural layered composite ceramic was fabricated by a tape-casting method. In the composite ceramics, the quaternary piezoelectric ceramic system $0.90Pb(Zr_{0.48}Ti_{0.52})O_3 - 0.05Pb(Mn_{1/3}Sb_{2/3})O_3 - 0.05Pb(Zn_{1/3}Nb_{2/3})O_3$ $(0.90PZT - 0.05PMS - 0.05PZN)$ was selected as the functional piezoelectric ceramic, and Al_2O_3-based ceramic was selected as the structural ceramic. Although the sintering temperature of pure Al_2O_3 ceramic is up to 1650 °C, which is much higher than that of the piezoelectric ceramic component, we realized the reduction of the sintering temperature for Al_2O_3 by adding a certain amount of sintering aids (Bi_2O_3, SiO_2 and B_2O_3). Moreover, excellent electrical and mechanical properties can be obtained in this functional and structural integrated composite ceramics by controlling the solid content, debinding and sintering process.

Experimental materials and methods

The starting materials selected for PZT-based piezoelectric ceramic were PbO (99.9%, 0.5 μm, $\rho = 9.53$ g/cm^3), ZrO_2 (99.99%, 100 nm, $\rho = 5.89$ g/cm^3), TiO_2 (99%, 100 nm, $\rho = 3.90$ g/cm^3), MnO_2 (99.99%, 0.5 μm, $\rho = 5.02$ g/cm^3), Sb_2O_3 (99.99%, 100 nm $\rho = 5.20$ g/cm^3), ZnO (99.99%, 100 nm, $\rho = 5.606$ g/cm^3) and Nb_2O_5 powder (99.99%, 30 nm, $\rho = 4.47$ g/cm^3). The main raw materials selected for Al_2O_3-based structural ceramic were Al_2O_3 (α-Al_2O_3, 99.99%, 30 nm, $\rho = 3.968$ g/cm^3), Bi_2O_3 (99.9%, 0.5 μm, $\rho = 8.90$ g/cm^3), SiO_2 (99.99%, 2 μm, $\rho = 2.60$ g/cm^3) and B_2O_3 (99.9%, 2 μm, $\rho = 2.46$ g/cm^3), and all of the reagents were purchased from Aladdin. The built-in electrodes were selected as EL44 − 040 Ag/Pd (70/30) electrodes.

The formula of piezoelectric ceramic was $0.90Pb(Zr_{0.48}Ti_{0.52})O_3 - 0.05Pb(Mn_{1/3}Sb_{2/3})O_3 - 0.05Pb(Zn_{1/3}Nb_{2/3})O_3$. The raw materials (PbO, ZrO_2, TiO_2, MnO_2, Sb_2O_3, ZnO and Nb_2O_5) were accurately weighed and ball-milled for 12 h in ethanol medium, and $0.90PZT - 0.05PMS - 0.05PZN$ ceramic powder was synthesized at 850 °C by the conventional solid-state reaction method. The evenly mixed piezoelectric ceramic powder was dispersed for 4 h in an anhydrous ethanol/butanone mixture solution with corn oil as the dispersant. Then, a binder (polyvinyl butyral) and a plasticizer (dibutyl phthalate) were added for the second grinding (8 h) to make the

powder particles uniformly coated by the organics, forming a stable and well-flowing slurry. Finally, the slurry is vacuumized to an appropriate viscosity. A dense, smooth and flexible green tape was formed by tape-casting the slurry.

Bi_2O_3, SiO_2 and B_2O_3 are used as the sintering additives to reduce the sintering temperature of alumina [16, 17]. The optimal mass ratio of Al_2O_3, Bi_2O_3, SiO_2 and B_2O_3 was confirmed as 6:2:1:1. The mixtures were ground for 12 h and then dried and sifted to obtain well-mixed powders. The preparation process of alumina green tape is similar to that of the PZT-based piezoelectric ceramic.

The dried green tapes were cut into disks with a diameter of 13 mm, and laminated (20 layers each), and the cast flakes with built-in electrodes were placed between the PZT green sheet and the alumina green sheet. The samples were placed into a die, stacked neatly for hot pressing at 70 °C and 15 MPa, and the pressure was maintained for 60 min. Then, pressed multilayers were sintered to obtain the composite ceramics according to the preset heating curves.

The radial shrinkage ratio R_s of the sample was calculated according to the formula:

$$R_s = (d_0 - d)/d_0 \times 100\% \qquad (1)$$

where d_0 is the diameter of the green tape before firing; d is the diameter of the sintered sample. Scanning electron microscope (SEM; Quanta 200, FEI) was used to observe the interface microstructure of the composite ceramic. For PZT layer polarizing and electric measuring of the composite ceramics, the inner electrode is extended out to the surface through a pin hole in alumina layer. Ferroelectric tester (multiferroic 100, Radiant Technologies) was adopted to test the ferroelectric properties. Quasi-static d_{33} tester (ZJ-3A, Institute of Acoustics of The Chinese Academy of Sciences) was used to measure the piezoelectric coefficient of the samples. The relative dielectric constant ε_r and dielectric loss $\tan\delta$ were analyzed by impedance analyzer (HP4294A, Agilent). The Vickers hardness test was conducted on the instrument of HVS-50 (Ningbo KECHENG Instrument Co., Ltd.).

Results and discussion

The solid contents of cast slurries are critical to the formation of continuous and dense tape-casting films as well as the linear shrinkage matching between PZT and alumina layers. According to the laws of fluid rheology, the distance between the solid particles gradually decreases with the increase in the solid content of the slurry, which accords with the Woodcock relationship [18]:

$$frachd = \left(\frac{1}{3\pi\phi} + \frac{5}{6}\right)^{1/2} - 1 \qquad (2)$$

where h is the distance between solid particles, d is the grain diameter, and Φ is the solid content. Based on the above equation, with the increase in solid content, the distance between the particles decreases and the organic binder is benefited to form a network structure among the ceramic particles. However, the particles in the slurry may form a continuous state and lose their fluidity once the solid content is over a certain value. Hence, in the case of over high solid content, the cast slurry is hard to form a continuous tape-casting film or the film cannot reach its required strength [19]. On the other hand, the ceramic will leave more holes after sintering and reduce the density if the solid content of the slurry is too low.

Figure 1 shows the linear shrinkage ratio of the green tapes with different solid contents of PZT- and Al_2O_3-based ceramics after sintered at 1150 °C for 4 h. For both ceramics, a nearly linear decreasing shrinkage can be seen with the increase in solid content. Furthermore, PZT-based ceramic presents a
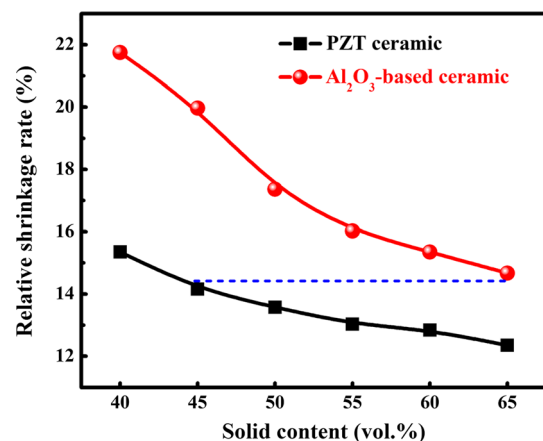
Figure 1 Linear shrinkage of sintered PZT- and Al_2O_3-based ceramics with different solid contents.

smaller shrinkage at the same solid content. At solid content of 45 vol.%, PZT shrinkage rate is 13.23%, while the solid content of alumina is 65% vol.%, and its shrinkage rate is 13.37%. Therefore, by adjusting the solid content, the shrinkage of the two ceramic components can be effectively matched so that the warpage and deformation caused by shrinkage mismatch in the sintering process can be avoided.

To confirm the temperature dependence of shrinkage and to optimize the sintering temperature, piezoelectric sample with starting solid content of 45 vol.% and alumina sample with starting solid content of 65 vol.% were compared by sintering the ceramics for 4 h in temperature range of $1050 \sim 1200$ °C. The observed results of radial shrinkage of piezoelectric ceramic and alumina ceramic samples are shown in Fig. 2. It can be seen that the radial shrinkage of both ceramics increases monotonically with the increase in sintering temperature, indicating an improved densification due to gradual growth of grain and reduction in the closed pores around the grain boundaries [20]. The variation range of the radial shrinkage rate of the piezoelectric ceramic is $9.57\% \sim 15.03\%$, while the variation range of the radial shrinkage rate of the alumina ceramic is $7.65\% \sim 16.96\%$ during sintering temperatures of $1050 \sim 1200$ °C. The radial shrinkage difference between the two ceramics is only 0.51% at sintering temperature of 1150 °C. In addition, the piezoelectric ceramic and the structural Al_2O_3-based ceramic can reach high density at this sintering temperature. It also needs to mention that the observed higher shrinkage of Al_2O_3-based ceramic at higher sintering temperature is mainly from
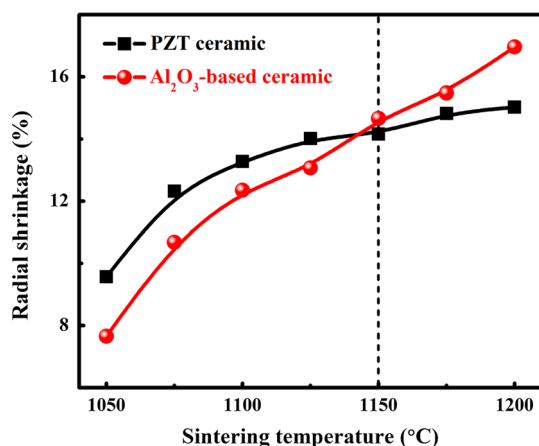
the loss of the low melting additives and the densification could not be further improved. Hence, the optimal co-sintering temperature was set at 1150 °C for the ceramic composites.

The density and grain morphology of the ceramic directly affect the electrical and mechanical properties of ceramic composites. Figure 3 shows the SEM images of the piezoelectric layer of the ceramic composites at different sintering temperatures. As can be seen in Fig. 3a, when the co-fired temperature is 1050 °C, the piezoelectric layer shows small grain size and obvious pores. With the increase in sintering temperature, the grains of piezoceramic layer grow up evenly as well as the porosity decreases obviously. When the temperature rises to 1150 °C, as shown in Fig. 3c, the piezoceramic layer reaches a dense state with almost uniform grain sizes around $2 \sim 3$ µm and much clearer grain boundaries. When the sintering temperature is up to 1200 °C, abnormal grain growth can be seen in the microstructure in Fig. 3d, resulting in uneven grain sizes and correspondingly poor electrical properties of the piezoceramic layer.

The interfacial microstructures between different components are critical to the comprehensive properties of the ceramic composites. Figure 4 shows the cross sections of SEM micromorphologies of the composite ceramics sintered for 4 h at temperatures of $1050 \sim 1200$ °C, in which the upper layer is piezoceramic layer, and the bottom layer is alumina ceramic layer. The middle layer with thickness of $5 \sim 6$ µm is the built-in inner electrode layer, which is indispensable to the measurement and utilization of the piezoelectric response of the piezoceramic layer. The cross-sectional SEM images illustrate that interface microstructures are also closely dependent on the sintering temperature. As shown in Fig. 4c, the piezoelectric layer reaches the state of densification at sintering temperature of 1150 °C, which is consistent with the observation in Fig. 3. Meanwhile, it displays sharp and clear interfaces between PZT-based piezoceramic/Ag − Pd inner electrode/Al_2O_3 ceramic layer in the composites. No obvious interface reactions are observed between these different layers, indicating the piezoelectric component, the inner electrode component and the alumina component have excellent co-sintering compatibility. On the other hand, the bottom Al_2O_3 layer also presents a dense microstructure at sintering temperature of 1150 °C, verifying that Bi_2O_3, SiO_2 and B_2O_3 additives effectively decreased the sintering temperature of

Figure 2 Radial shrinkage of piezoelectric ceramic and alumina ceramic sintered at different temperatures for 4 h.

Figure 3 SEM images of composite ceramic piezoelectric layer: **a** 1050 °C, **b** 1100 °C, **c** 1150 °C and **d** 1200 °C.
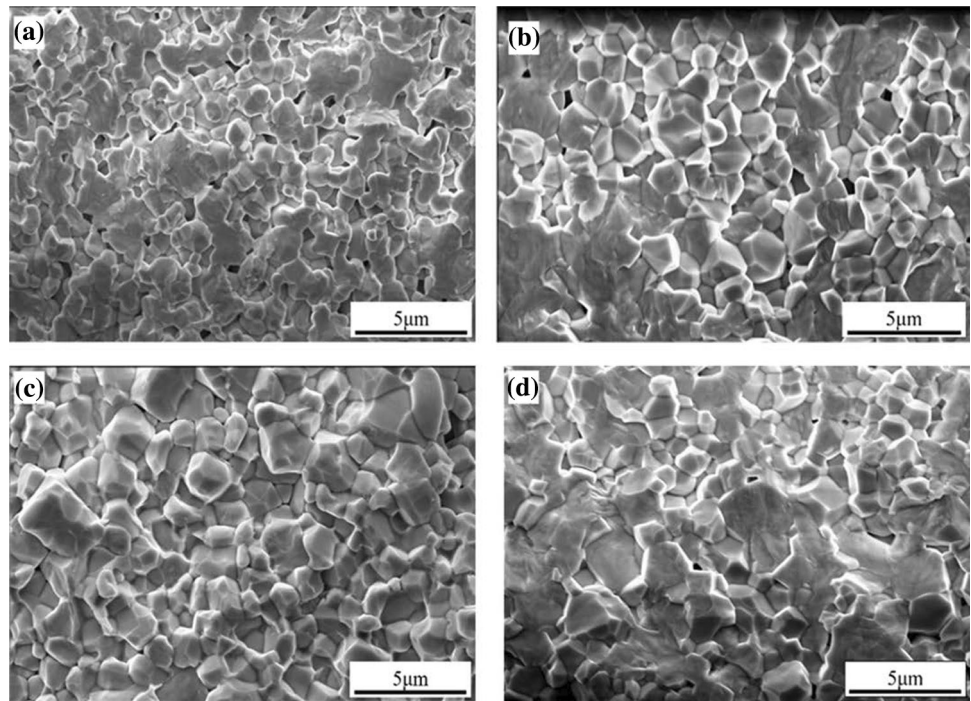
Figure 4 SEM images of a cross section of a composite ceramic: **a** 1050 °C, **b** 1100 °C, **c** 1150 °C and **d** 1200 °C.
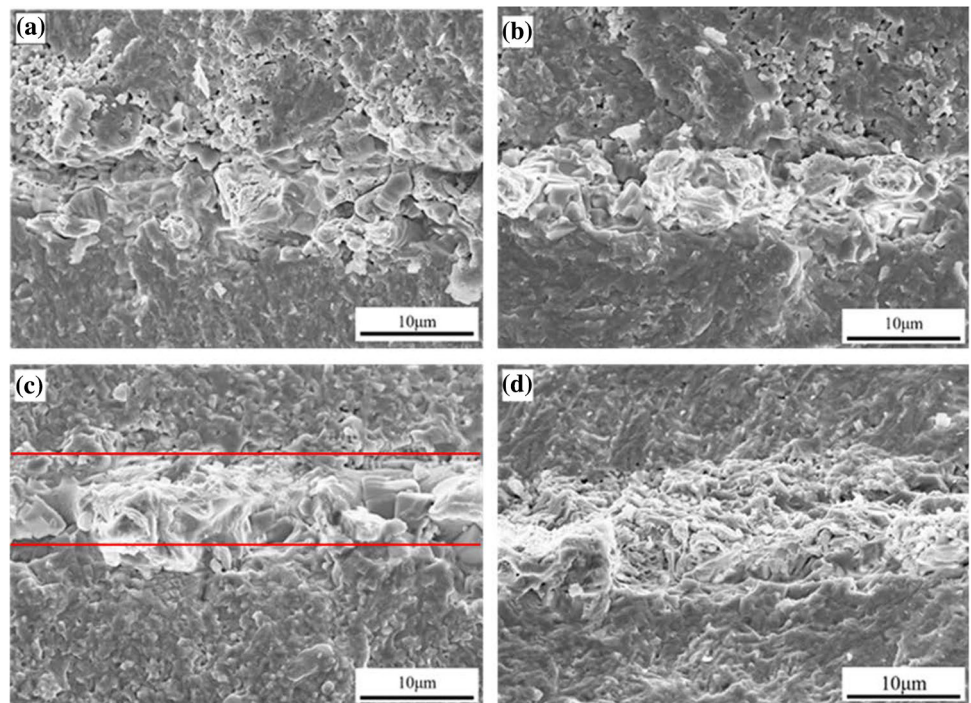

Al_2O_3 to assist a full densification [18]. When the sintering temperature is up to 1200 °C, as shown in Fig. 4d, the piezoelectric and alumina layers remain in a densification state. However, the diffusion of Ag − Pd inner electrode layer is more serious and leads to a blurred interface boundary and an extension in interface dimension. Cavities and even fractures occur that could be induced in the inner electrode because of interface diffusion [19, 20]. Therefore, in order to achieve the co-fired preparation of the layered ceramic composites, control of the
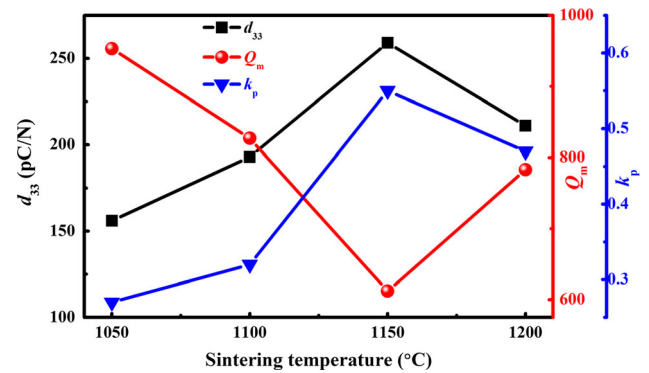
compositions of every single layer and control of the sintering temperature are extremely prerequisite.

The sintering temperature is decisive to the microstructures and interface diffusions. Hence, it also effectively impacts on the electrical properties of composite materials. Figure 5 shows the dielectric coefficient ε_r and dielectric loss $\tan\delta$ of the piezoceramic layer in PZT/Al$_2$O$_3$ composites sintered at different temperatures. The curves present that ε_r of the piezoceramic layer increases first and then decreases with the increase in sintering temperature, while $\tan\delta$ decreases first and then increases. Higher densification and larger grain with uniform size will be beneficial to the dielectric properties of the piezoelectric ceramic [21]. At sintering temperature of 1150 °C, optimal dielectric properties with maximum dielectric constant of 965 and minimum dielectric loss of 0.37% were obtained in the piezoceramic layer. It is understandable that the piezoceramic layer displays dense microstructure as well as tightly and evenly arranged grains at this sintering temperature, as discussed in Fig. 3c. When the sintering temperature is higher than 1150 °C, decrease in dielectric constant and increase in dielectric loss were observed from the piezoceramic layer. Except the abnormal grain growth shown in Fig. 3d, interface diffusion and doping effects such as the immigrated Bi^{3+} into PZT-based piezoelectric layer are also responsible for the degradation in dielectric properties [22]. EDS analysis confirmed that PZT layer of the composite ceramic incorporated nearly 10 atm% Bi^{3+} ions because of the interface diffusion when sintering at 1200 °C.

Figure 6 shows the piezoelectric coefficient d_{33}, electromechanical coupling factor k_p and mechanical quality factor Q_m of the piezoceramic layer in PZT/
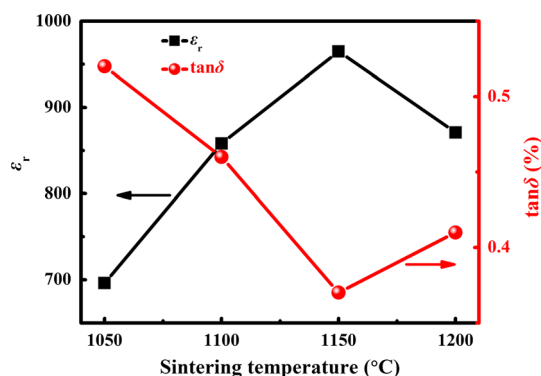
Figure 6 The d_{33}, Q_m and k_p of composite ceramic piezoelectric layer with sintering temperatures.

Al$_2$O$_3$ composites prepared at different sintering temperatures. According to the figure, with the increase in sintering temperature, d_{33} and k_p of the piezoelectric layer first increase and then decrease. When the sintering temperature is 1150 °C, d_{33} and k_p are 259 pC/N and 0.55, respectively. This tendency in piezoelectric properties is similar to the dependence of the dielectric properties on the sintering temperature. The optimal piezoelectric properties are also attributed to the optimized microstructures, crystal structures and composition control in suitable sintering temperature. On the other hand, the sintering defects, lattice distortions, oxygen vacancies and space charges induced by doping effects and grain boundaries will pin the domain wall and restrict the movement of the domain wall, making domains difficult to orientation, leading to enhancement in Q_m and reduction in the piezoelectric coefficient [23, 24]. Hence, it is usual that Q_m shows opposite tendency with that of d_{33} and k_p in piezoelectric materials.

Table 1 shows the hardness values of the Al$_2$O$_3$ structural layer in the ceramic composites sintered at different temperatures. At sintering temperature of 1050 °C, the hardness of the alumina layer is 615 HV. With the increase in sintering temperature, the hardness of the alumina layer increases gradually. The improved hardness with the rising of sintering temperature is mainly attributed to the promotion in densification of alumina layer [25]. The hardness of the alumina layer is up to 667 HV at sintering

Figure 5 The ε_r and $\tan\delta$ of piezoceramic layer in composites sintered at different temperatures.

Table 1 Hardness values of composite ceramic alumina layers

Co-firing temperature (°C)	1050	1100	1150	1200
Hardness (HV)	615	640	667	680

temperature of 1150 °C. For the layered functional/structural composites, this mechanical property is satisfied for many application occasions, e.g., the full-ceramic piezoelectric actuators.

Conclusions

In conclusion, the sintering temperature of Al_2O_3-based structural ceramic was effectively reduced by adding sintering aids in Al_2O_3 powder. Then, the mismatching in sintering shrinkage of the different components in ceramic composites was solved by adjusting the solid content and co-fired temperature of the cast slurry. At last, layered piezoelectric/structural ceramic composites with excellent interface bonding and high density were successfully obtained by co-fired preparation at 1150 °C sintering temperature. The dielectric constant and dielectric loss of the piezoelectric layer are 965 and 0.37%, respectively, and the piezoelectric constant is 259 pC/N. Moreover, the structural layer of the layered ceramic composites presents good mechanical property with hardness of 667 HV. The developed piezoelectric/structural ceramic composites could be beneficial to the utilization in the full-ceramic devices.

Acknowledgements

References

[1] Ryu JH, Carazo AV, Uchino K, Kim HE (2001) Magneto-electric properties in piezoelectric and magnetostrictive laminate composites. Jpn J Appl Phys 40:4948–4951. https://doi.org/10.1143/JJAP.40.4948

[2] Sglavo VM, Bertoldi M (2006) Design and production of ceramic laminates with high mechanical resistance and reliability. Acta Mater 54(18):4929–4937. https://doi.org/10.1016/j.actamat.2006.06.019

[3] Peng R, Li Y, Lu Y, Yun Y, Du W, Tao Z, Liao B (2020) High-performance microwave dielectric composite ceramics sintered at low temperature without sintering-aids. J Alloy Compd 831:154878. https://doi.org/10.1016/j.jallcom.2020.154878

[4] Chawla KK (2013) Ceramic matrix composites. Springer Science & Business Media, New York

[5] Coelho PG, Guedes JM, Rodrigues HC (2015) Multiscale topology optimization of bi-material laminated composite structures. Compos Struct 132:495–505. https://doi.org/10.1016/j.compstruct.2015.05.059

[6] Kiyono CY, Silva ECN, Reddy JN (2016) Optimal design of laminated piezocomposite energy harvesting devices considering stress constraints. Int J Numer Meth Eng 105(12):883–914. https://doi.org/10.1002/nme.4996

[7] Sinchuuk Y, Piat R, Roy S, Gibmeier J, Wanner A (2011) Inelastic behavior of the single domain of metal-ceramic composites with lamellar microstructure. Pamm 11(1):285–286. https://doi.org/10.1002/pamm.201110134

[8] Zhao CP, Fang F, Yang W (2010) A dual-peak phenomenon of magnetoelectric coupling in laminated Terfenol-D/PZT/Terfenol-D composites. Smart Mater Struct 19(12):125004. https://doi.org/10.1088/0964-1726/19/12/125004

[9] Akedo J (2008) Room temperature impact consolidation (RTIC) of fine ceramic powder by aerosol deposition method and applications to microdevices. J Therm Spray Technol 17(2):181–198. https://doi.org/10.1007/s11666-008-9163-7

[10] Baba S, Akedo J (2009) Fiber laser annealing of nanocrystalline PZT thick film prepared by aerosol deposition. Appl Surf Sci 255(24):9791–9795. https://doi.org/10.1111/j.1551-2916.2006.01030.x

[11] Akedo J (2006) Aerosol deposition of ceramic thick films at room temperature: densification mechanism of ceramic layers. J Am Ceram Soc 89(6):1834–1839. https://doi.org/10.1111/j.1551-2916.2006.01030.x

[12] Fernie JA, Roberts MD, Wang Y, Kavilveedu NR, Brown D (2015) Double transition joint for the joining of ceramics to metals. US patent. US9011620

[13] Hu F, Liu W, Xie Z (2016) Surface modification of alumina powder particles through stearic acid for the fabrication of translucent alumina ceramics by injection molding. Ceram Int 42(14):16274–16280. https://doi.org/10.1016/j.ceramint.2016.07.164

[14] Jian G, Hu Q, Lu S, Zhou D, Fu Q (2012) Effect of solid content variations on PZT slip for tape casting. Process Appl Ceram 6(4):215–221. https://doi.org/10.2298/PAC1204215J

[15] Cristofolinia I, Raob A, Menapace C, Molinarib A (2010) Influence of sintering temperature on the shrinkage and geometrical characteristics of steel parts produced by powder metallurgy. J Mater Process Tech 210(13):1716–1725. https://doi.org/10.1016/j.jmatprotec.2010.06.002

[16] Qin Y, Zhong CW, Yang HY et al (2019) Enhanced thermal and mechanical properties of Li–Al–Si composites with

K2O–B2O3–SiO2 glass for LTCC application. Ceram Int 45:15654–15659. https://doi.org/10.1016/j.ceramint.2019.05.077

[17] Zhou XH, Ning XQ, Zhang X et al (2020) Influence of Li2O–MgO–ZnO–B2O3–SiO2 glass doping on the microwave dielectric properties and sintering temperature of Li3Mg2NbO6 ceramics. J Mater Sci Mater Electron 31:17029–17035. https://doi.org/10.1007/s10854-020-04260-3

[18] Bhuyan RK, Kumar TS, Pamu D (2017) Liquid phase effect of Bi_2O_3 additive on densification, microstructure and microwave dielectric properties of Mg_2TiO_4 ceramics. Ferroelectrics 516(1):173–184. https://doi.org/10.1080/00150193.2017.1362226

[19] Zuo R, Li L, Gui Z (2001) Relationships between interfacial interaction, electrode formulation and cofiring mismatch of relaxor-based multilayer ceramic devices. J Mater Sci Mater Electron 12(2):117–121. https://doi.org/10.1023/A:1011258321843

[20] Lin JC, Chan JY (1996) On the resistance of silver migration in Ag-Pd conductive thick films under humid environment and applied dc field. Mater Chem Phys 43(3):256–265. https://doi.org/10.1016/0254-0584(95)01642-8

[21] Yoo JH, Kim SW, Lee ES, Choi NG, Jeong HS (2019) Microstructure and piezoelectric properties of PMN-PNN-PZT ceramics with the variation of PMN. Trans Electron Electron Mater 20(1):31–35. https://doi.org/10.1007/s42341-018-00088-1

[22] Zhang Y, Zhu X, Zhu J, Zeng X, Feng X, Liao J (2016) Composition design, phase transitions and electrical properties of Sr2+-substituted xPZN–0.1 PNN–(0.9–x) PZT piezoelectric ceramics. Ceram Int 42(3):4080–4089. https://doi.org/10.1016/j.ceramint.2015.11.080

[23] Omran KH, Abd El-sadek MS, Mostafa M, Hemeda OM (2020) Influence of PbO phase content on structural and optical properties of PZT nanopowders. Appl Nanosci 10(7):2315–2327. https://doi.org/10.1007/s13204-020-01390-2

[24] Mao Y, Banerjee S, Wong SS (2003) Hydrothermal synthesis of perovskite nanotubes. Chem Commun 3(3):408–409. https://doi.org/10.1039/B210633G

[25] Jiang XS, Wang NJ, Zhu DG (2014) Friction and wear properties of in-situ synthesized Al_2O_3 reinforced aluminum composites. Trans Nonferr Metals Soc China 24(7):2352–2358. https://doi.org/10.1016/S1003-6326(14)63356-2

Springer